ACS OMEGA

Open Access



http://pubs.acs.org/journal/acsodf

Article

# Analogues of Dihydroflavonol and Flavone as Protein Tyrosine Phosphatase 1B Inhibitors from the Leaves of *Artocarpus elasticus*

Abdul Bari Shah, Aizhamal Baiseitova, Gihwan Lee, Jeong Ho Kim, and Ki Hun Park*

Cite This: *ACS Omega* 2024, 9, 9053−9062

Read Online

ACCESS | Metrics & More | Article Recommendations | Supporting Information

**ABSTRACT:** Protein tyrosine phosphatase 1B (PTP1B) is one of the target enzymes whose disruption leads to obesity and diabetes. A series of PTP1B inhibitors were isolated from the leaves of *Artocarpus elasticus*, used in traditional medicines for diabetes. The isolated inhibitors (**1**−**13**), including two new compounds (**1** and **2**), consisted of dihydroflavonols and flavones. The structural requirements for the PTP1B inhibitory mode and potency were revealed in both skeletons. The two highest PTP1B inhibitory properties were dihydroflavonol **1** and flavone **6** analogs with $IC_{50}$ values of 0.17 and 0.79 $\mu$M, respectively. The stereochemistry also affected inhibitory potencies: *trans* isomer **1** ($IC_{50}$= 0.17 $\mu$M) vs *cis* isomer **2** ($IC_{50}$= 2.24 $\mu$M). Surprisingly, the dihydroflavonol and flavone glycosides (**11** and **13**) displayed potent inhibition with $IC_{50}$s of 2.39 and 0.22 $\mu$M, respectively. Furthermore, competitive inhibitor **1** was applied to time-dependence experiments as a simple slow-binding inhibitor with parameters of $K_i^{app}$ = 0.064103 $\mu$M, $k_3$ = 0.2262 $\mu M^{-1}$ $min^{-1}$, and $k_4$ = 0.0145 $min^{-1}$. The binding affinities by using the fluorescence quenching experiment were highly correlated with inhibitory potencies: **1** ($IC_{50}$= 0.17 $\mu$M, $K_{SV}$ = 0.4375 × $10^5$ L·$mol^{-1}$) vs **3** ($IC_{50}$= 17.79 $\mu$M, $K_{SV}$ = 0.0006 × $10^5$ L·$mol^{-1}$). The specific binding interactions were estimated at active and allosteric sites according to the inhibitory mode by molecular docking.

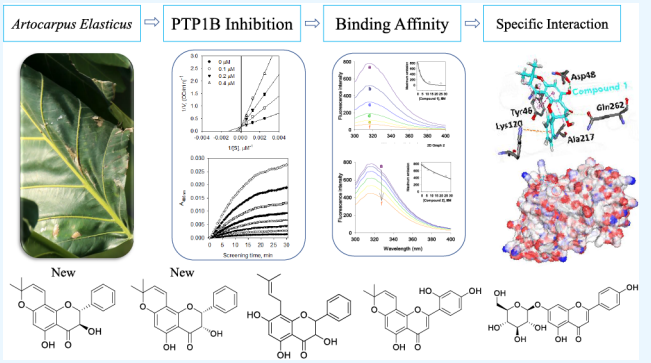


## 1.. INTRODUCTION

Protein tyrosine phosphatase 1B (PTP1B) is a negative regulator of insulin signaling pathways, causing insulin resistance. Insulin signaling is initiated by the phosphorylation of insulin receptor (IR) and insulin receptor substrate (IRS). Sequentially, these phosphorylations activate many signaling cascades resulting in several biological responses like the transport of glucose into the cells and synthesis of glycogen.[1,2] PTP1B blocks this signaling pathway through the dephosphorylation of IR and IRS, making PTP1B a viable therapeutic target in the treatment of type 2 diabetes (T2DM).[3] In addition, improved insulin signaling in PTP1B knockout mice indicates that this enzyme is a key factor in the regulation of insulin sensitivity.[4] PTP1B is extensively expressed in various organs, including the fat, muscle, and liver.[5] Additionally, PTP1B levels appear to be elevated in some physiological or pathological contexts of leptin resistance, which is connected to food intake leading to obesity.[6] Thus, PTP1B inhibitors may be considered as excellent lead compounds for the treatment of obesity and diabetes.

*Artocarpus elasticus* belongs to the Moraceae family and is commonly known as terap. It is found in Malaysia, Pacific Islands, India, North Australia, and Central America. Most parts of terap, including fruit, leaves, and bark, have been used in traditional medicines due to its antimicrobial, anti-inflammatory, and hypoglycemic effects.[7,8] The metabolic study of this plant has been intensively focused on roots and barks. The most abundant metabolites in both these parts were found to be prenylated flavonoids and dihydrobenzoxanthones with diverse biological activities. For example, the prenylated flavonoids showed antioxidant, cytotoxic, tyrosinase, and 5-$\alpha$ reductase inhibitory activities, while dihydrobenzoxanthones exhibited $\alpha$-glucosidase, human neutrophil elastase, and bacterial neuraminidase inhibitory activities.[7−14] The ripened leaves of terap are dried, grounded, and used for preparing tea, which is effective in preventing chronic diseases such as diabetes, hypertension, and malaria.[15−18] But there are only two influential reports about their metabolites, which deal with alkylated dihydrochalcones.[7,15] Those compounds were not effective for PTP1B inhibition in our preliminary work. This encouraged us to conduct metabolite investigation targeting PTP1B inhibition.

The aim of this study was to investigate the responsible metabolites for PTP1B inhibition from the leaves of *A.*

Received: October 3, 2023
Revised: December 18, 2023
Accepted: February 1, 2024
Published: February 14, 2024

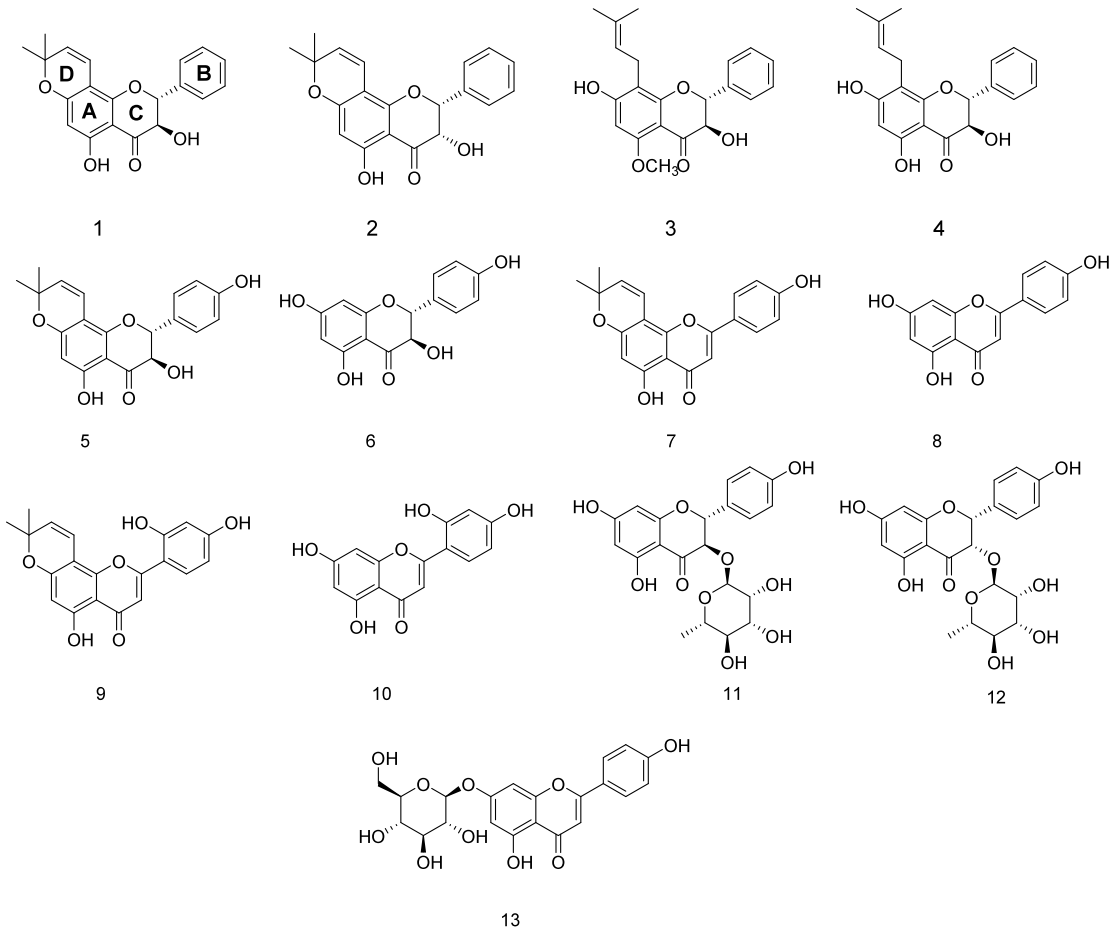


**Figure 1.** Structure of bioactive compounds (**1**−**13**) isolated from *Artocarpus elasticus* leaves.

*elasticus*. A series of isolated compounds were applied to the PTP1B enzyme to disclose inhibitory potencies, behavior, and activity relationship of structural features. The specific binding interaction was predicted by molecular docking.

## 2.. RESULTS AND DISCUSSION

**2.1.. Structural Elucidation.** In the course of exploring the PTP1B inhibitor, the methanol extract of *A. elasticus* leaves displayed potent inhibition with 80% inhibition at 50 $\mu$g/mL concentration. This encouraged us to examine PTP1B inhibitory metabolites from the leaves of this species. The crude methanol extract was fractionated by liquid−liquid fractionation method with solvents having different polarities, namely, hexane, chloroform, ethyl acetate, and water. Then, repeated liquid chromatography separations of the chloroform fraction using MPLC and recycled HPLC resulted in 13 phenolic compounds. Their structures (as shown in Figure 1) were elucidated by their spectroscopic data (Figures S1−S49 and Table S1) and compared with those of previous reports. The isolates (**3**−**13**) were identified as artoscortonol[19] (**3**), glepidotin B[20] (**4**), yukovanol[21] (**5**), dihydrokaempferol[22] (**6**), atalantoflavone[23] (**7**), apigenin[24] (**8**), 2′-hydroxyatalantoflavone[25] (**9**), norartocarpetin[10] (**10**), engeletin[26] (**11**), isoengeletin[26] (**12**), and apigenin-7-*O*-$\beta$-D-glucopyranoside[27] (**13**). Compounds **1** and **2** were found to be new dihydroflavonols.

Compound **1** obtained as a yellowish solid, $[\alpha]^{20}_{D}$ −5.33 (c 0.1, MeOH), had a molecular formula $C_{20}H_{18}O_5$ established by the $[M + H]^+$ ion at 339.1232 (calcd 338.1154) in the HR−ESI−MS (Figure S8). The IR spectrum of **1** exhibited absorption at 3472, 2980, and 1628 cm$^{-1}$. The dihydroflavonol motif was assumed from the presence of a pair of doublets at $\delta_H$ 4.69 (1H, dd, $J$ = 11.5 Hz, H-3) and 5.25 (1H, d, $J$ = 11.5 Hz, H-2), as well as a singlet of chelated −OH at $\delta_H$ 11.76 in $^1$H NMR spectrum (Table 1 and Figure S1). The pyran group fixed with an A-ring was established from AB coupling of H-1″($\delta_H$ 6.45, 1H, d, $J$ = 10.1 Hz) and H-2″($\delta_H$ 5.60, 1H, d, $J$ = 10.1 Hz) and HMBC correlation between H-4″($\delta_H$ 1.42) and oxygenated carbon C-7 ($\delta_C$ 157.7). The position of the pyran ring was confirmed by the HMBC correlation of H-2″($\delta_H$ 5.60) to C-8 ($\delta_C$ 102.7). The monosubstituted B-ring was easily deduced by H-2′/6′($\delta_H$ 7.62, 2H), H-3′/5′($\delta_H$ 7.42, 2H), and H-4′($\delta_H$ 7.42, m) (Figures 2 and S7). The stereochemistry of C-2 was confirmed as R configuration by CD spectra with a positive Cotton effect at 326 nm and a negative effect at 302 nm[28] (Figure S50). The *trans* relationship between C-2 and C-3 was deduced by coupling constant ($J$ = 11.5 Hz) and NOESY relationship (Figures 2 and S5). Thus, compound **1** was identified as (2*R*,3*R*)-3,5-dihydroxy-8,8-dimethyl-2-phenyl-2,3-dihydro-4H,8H-pyrano-[2,3-*f*]chromen-4-one, namely yukovanol A.

Compound **2** obtained as yellowish solid, $[\alpha]^{20}_{D}$ − 26.7 (c 0.1, MeOH), had a molecular formula $C_{20}H_{18}O_5$ established by the $[M + H]^+$ ion at 339.1232 (calcd 338.1154) in the HR−ESI−MS (Figure S16). The IR spectrum of compound **2** exhibited absorption at 3472, 2980, and 1628 cm$^{-1}$. Its $^1$H, $^{13}$C, and 2D NMR data (Table 1 and Figures S9−S15) closely resembled compound **1**, and thus predicted as diastereomers of


https://doi.org/10.1021/acsomega.3c07471
ACS Omega 2024, 9, 9053−9062

Table 1. $^{1}$H and $^{13}$C NMR Spectroscopic Data ($\delta$ in ppm, $J$ in Hz) of 1 and 2 (acetone-$d_6$)

| | 1 | | 2 | |
|---|---|---|---|---|
| no | $\delta_H$ | $\delta_C$ | $\delta_H$ | $\delta_C$ |
| 2 | 5.25 (d, $J$ = 11.1) | 84.4 | 5.24 (d, $J$ = 3.6) | 84.3 |
| 3 | 4.69 (d, $J$ = 11.5) | 73.1 | 4.67 (dd, $J$ = 3.8, 11.6) | 73.1 |
| 4 | | 198.4 | | 198.3 |
| 4a | | 102.0 | | 101.9 |
| 5 | | 164.3 | | 164.2 |
| 6 | 5.94 (s) | 98.0 | 5.96 (s) | 98.0 |
| 7 | | 157.7 | | 157.6 |
| 8 | | 102.7 | | 102.7 |
| 8a | | 163.1 | | 163.1 |
| 1′ | | 138.1 | | 138.1 |
| 2′ | 7.62 (m) | 128.8 | 7.61 (m) | 128.7 |
| 3′ | 7.42 (m) | 129.1 | 7.41 (m) | 129.1 |
| 4′ | 7.42 (m) | 129.6 | 7.41 (m) | 129.6 |
| 5′ | 7.42 (m) | 129.1 | 7.41 (m) | 129.1 |
| 6′ | 7.62 (m) | 128.8 | 7.61 (m) | 128.7 |
| 1″ | 6.45 (d, $J$ = 10.1) | 115.8 | 6.44 (d, $J$ = 10.1) | 115.7 |
| 2″ | 5.60 (d, $J$ = 10.1) | 127.7 | 5.58 (d, $J$ = 10.1) | 127.7 |
| 3″ | | 79.1 | | 79.0 |
| 4″ | 1.42 (s) | 28.6 | 1.41 (s) | 28.6 |
| 5″ | 1.43 (s) | 28.4 | 1.43 (s) | 28.4 |

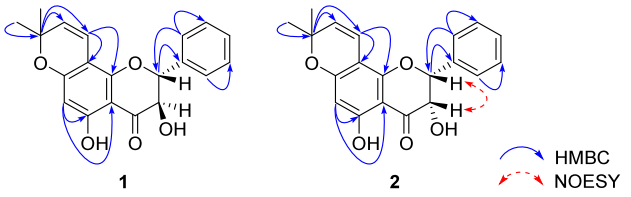


Figure 2. HMBC and NOESY correlation of compounds 1 and 2.

each other. The *cis* configuration was confirmed by a strong NOE between H-2 and H-3, and lower $J$-value ($\delta_H$ 5.24, 1H, d, $J$ = 3.6 Hz and $\delta_H$ 4.67, 1H, dd, $J$ = 3.8, 11.6 Hz) dissimilarity to compound **1** (Figures 2 and S13). The pattern of the Cotton effect was close to compound **1**. Thus, compound **2** was identified as (2*R*,3*S*)-3,5-dihydroxy-8,8-dimethyl-2-phenyl-2,3-dihydro-4H,8H-pyrano[2,3-*f*]chromen-4-one, namely yukovanol B.

**2.2.. PTP1B Inhibitory Activities of Isolated Compounds.** More detailed PTP1B inhibitory activities of the isolated compounds were subsequently conducted according to the established procedures.[29] As shown in Figure 3A and Table 2, all compounds displayed PTP1B inhibition with $IC_{50}$ values ranging between 0.17 and 35.4 $\mu$M dose dependently. The most potent inhibitor was found to be compound **1** ($IC_{50}$ = 0.17 $\mu$M), but the potency of these inhibitors was affected by subtle changes in their structure and stereochemistry. In the result of comparison of the inhibition activity between diastereomers **1** and **2**, *trans*-confirmation (**1**) was 13-fold more effective than the *cis* one (**2**). Their binding interaction with the enzyme at the active site was performed by molecular docking experiments (*Vida infra*). The hydroxyl group at C-4′(B-ring) led to a significant decrease in inhibitory potency: **1** vs **5** ($IC_{50}$ = 3.07 $\mu$M). The pyran motif in the A-ring would be a critical functionality to PTP1B inhibition: pyran **9** ($IC_{50}$ = 0.79 $\mu$M) vs **10** ($IC_{50}$ = 3.39 $\mu$M) and pyran **7** ($IC_{50}$ = 1.19 $\mu$M) vs **8** ($IC_{50}$ = 5.99 $\mu$M). Also, the pyran compound **5** was 9-fold effective than its mother compound **6** ($IC_{50}$ = 35.41 $\mu$M). It is a general expectation that glycoside motif functions to lessen the inhibitory potency.[30] However, glycosides of dihydroflavonol **11** ($IC_{50}$ = 2.39 $\mu$M) and flavone **13** ($IC_{50}$ = 0.22 $\mu$M) showed much better inhibitions than their mother skeletons (**6** and **8**) with 15-fold and 27-fold, respectively.

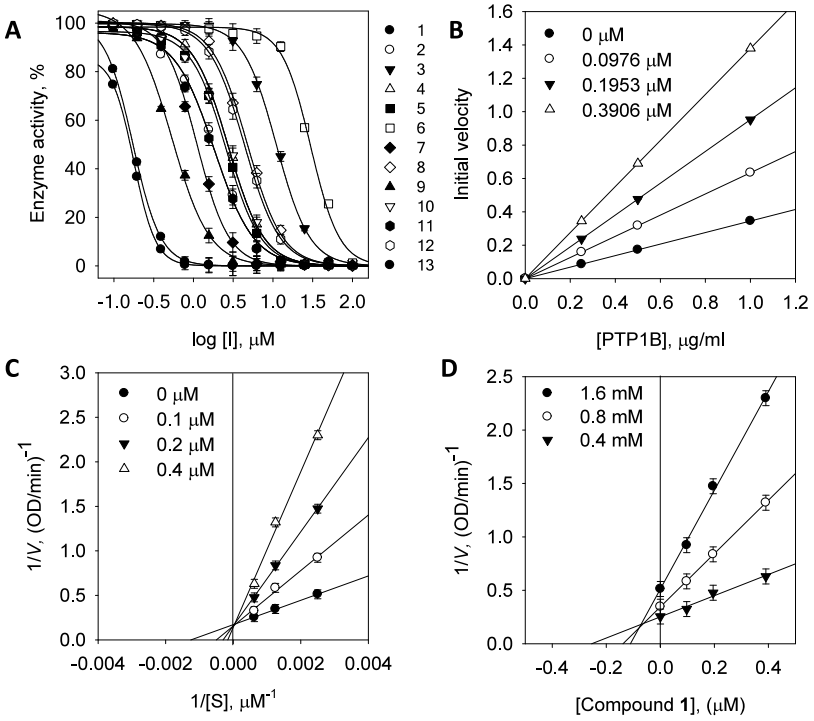


Figure 3. (A) Dose-dependent inhibition effect of compounds on PTP1B. (B) The catalytic activity of PTP1B as a function of enzyme concentration at different concentrations of compound **1**. (C) The Lineweaver−Burk and Dixon (D) plots for PTP1B inhibition of compound **1**.



https://doi.org/10.1021/acsomega.3c07471
ACS Omega 2024, 9, 9053−9062

**Table 2. Inhibitory Effects of Compounds 1−13 on PTP1B**

| | PTP1B | | | |
|---|---|---|---|---|
| compounds | $IC_{50}$ ($\mu$M)[a] | kinetic mode ($K_i$, $\mu$M)[b] | $K_I$ ($\mu$M) | $K_{IS}$ ($\mu$M) |
| **1** | 0.17 ± 0.3 | competitive (0.07 ± 0.1) | NT[c] | NT |
| **2** | 2.24 ± 0.5 | competitive (1.04 ± 0.2) | NT | NT |
| **3** | 17.79 ± 0.2 | competitive (8.08 ± 0.1) | NT | NT |
| **4** | 3.52 ± 0.4 | competitive (1.61 ± 0.2) | NT | NT |
| **5** | 3.07 ± 0.2 | noncompetitive (3.46 ± 0.3) | NT | NT |
| **6** | 35.41 ± 0.7 | noncompetitive (34.66 ± 0.8) | NT | NT |
| **7** | 1.19 ± 0.3 | competitive (0.45 ± 0.1) | NT | NT |
| **8** | 5.99 ± 0.5 | competitive (2.90 ± 0.3) | NT | NT |
| **9** | 0.79 ± 0.3 | mixed type I (0.58 ± 0.1) | 0.50 | 2.89 |
| **10** | 3.39 ± 0.2 | mixed type I (2.71 ± 0.2) | 2.68 | 5.23 |
| **11** | 2.39 ± 0.4 | mixed type I (1.16 ± 0.2) | 1.20 | 8.33 |
| **12** | 4.76 ± 0.5 | mixed type I (3.20 ± 0.3) | 3.19 | 9.55 |
| **13** | 0.22 ± 0.3 | mixed type I (0.18 ± 0.1) | 0.18 | 0.80 |
| ursolic acid[d] | 16.5 ± 0.8 | NT | NT | NT |

[a]Sample concentration which led to 50% enzyme activity loss. [b]$K_I$ is the inhibition constant. [c]NT is not tested. [d]Ursolic acid is used as a positive control.

### 2.3.. Inhibitory Kinetics of the Compounds to PTP1B.

The reversibility of the inhibitors to the enzyme was established by plotting the initial velocity as a function of the concentration of a representative compound **1** in Figure 3B. The resulting family of straight lines passing through the same origin implies the typical reversibility of the inhibitor to the enzyme. Moreover, the inhibitory behavior of the compounds was analyzed using Lineweaver−Burk plots, which revealed differences based on the compound's skeleton. In dihydroflavonols (**1**−**6**), a hydroxyl group on the B-ring attributed to the inhibitory behavior. Dihydroflavonols (**1**−**4**) in the absence of a hydroxyl group on the B-ring showed a typical competitive mode, in which there are no changes in $V_{max}$ and the increasing inhibitor concentration (Figure 3C).

Dihydroflavonols **5** and **6** with the 4-hydroxyl group on the B-ring exhibited a noncompetitive mode with decrease in $V_{max}$ and no change in the $K_m$ value (Figure 4A). Inhibitory modes were also affected by the B-ring in flavones (**7**−**10**). The flavones (**7** and **8**) with 4-hydroxyl on the B-ring inhibited PTP1B with the noncompetitive mode, but the flavones (**9** and **10**) with resorcinol motif on the B-ring showed mixed-type inhibitions. The three glycosides (**11**−**13**) showed a mixed-type inhibition in which the increasing inhibitor concentration caused the family of lines to shift to the left of the *y*-axis and above the *x*-axis, indicating a common intercept (Figure 4B). The parameters $K_I$ and $K_{IS}$ were fitted in eqs 2−4 to distinguish between two probable mechanisms of mixed-type inhibition (I or II). Our analysis indicated that all compounds had a higher $K_{IS}$ than $K_I$ and preferred binding with the free enzyme rather than the enzyme−substrate complex, which supports the mixed type I mode of inhibition against PTP1B. Finally, the $K_I$ values presented in Table 2 were estimated using Dixon plots, where the $K_I$ value of the most active inhibitor (**1**) was determined to be 0.07 $\mu$M (Figure 3D). The Lineweaver−Burk and Dixon plots of other compounds (**2**−**4**, **6**−**12**) are represented in Figures S51−S54.

Furthermore, we examined a time-dependent inhibitory phenomenon for the most effective inhibitor **1** displaying a competitive mode. A time-dependent analysis was achieved by evaluating the initial velocities of phosphate group hydrolysis with respect to the preincubation time of the enzyme with the inhibitor. The mixture of enzyme and inhibitor **1** was incubated in the time range of 0−75 min, where enzyme activity was not affected (Figure 5A inset). The residual enzyme activity was lowered gradually according to a function of preincubation time, which is a typical progress behavior of time dependence (Figure 5A).

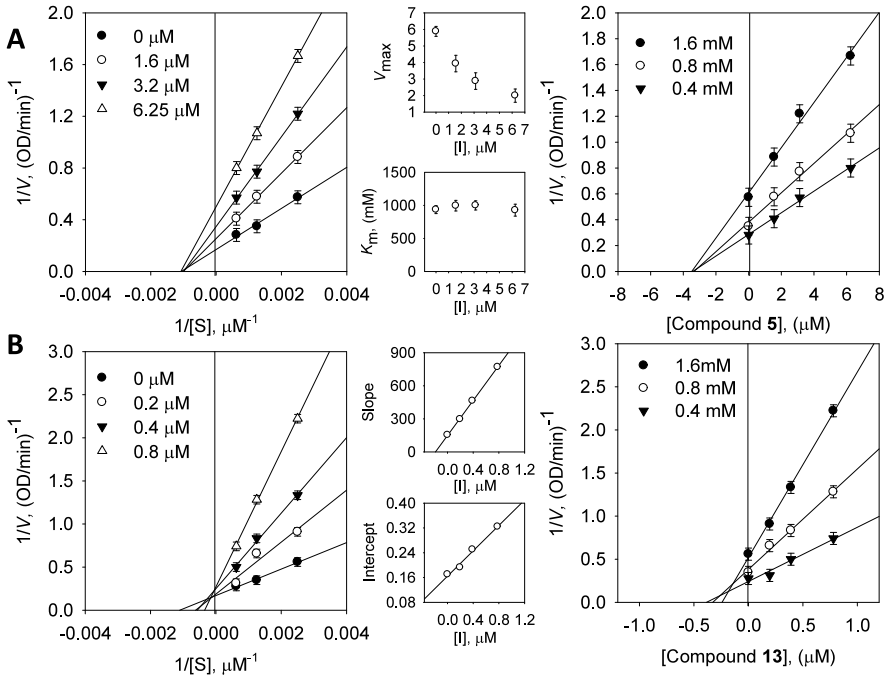


**Figure 4.** Lineweaver−Burk and Dixon plots for PTP1B inhibition of (A) compound **5** and (B) compound **13**.



https://doi.org/10.1021/acsomega.3c07471
ACS Omega 2024, 9, 9053−9062

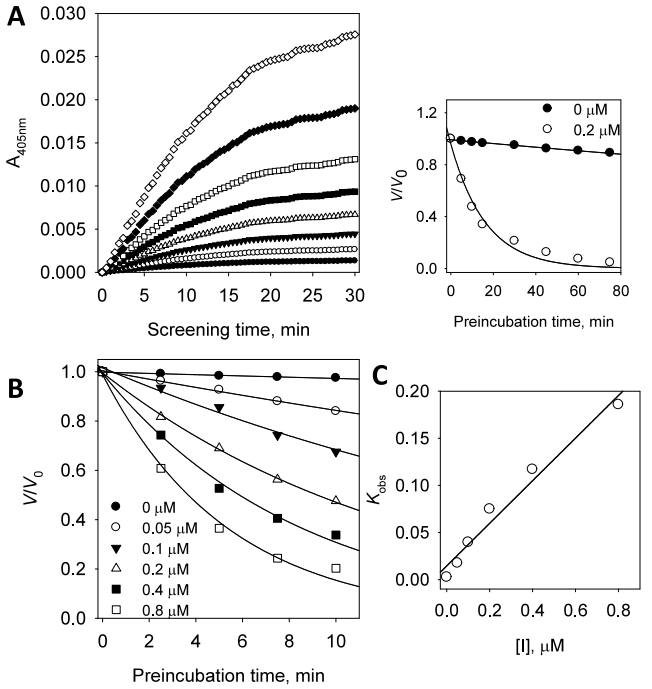


**Figure 5.** (A) Slow-binding inhibition at different preincubation times (◇: 0; ◆: 5; □: 10; ■: 15; △: 30; ▼: 45; ○: 60; ●: 75 min) for compound **1** at 0.2 $\mu$M. Inset: inhibition as a function of preincubation time for compound **1**. (B) Time course of the inactivation of PTP1B compound **1**. (C) plot of $k_{kobs}$ on the dependence on different concentrations of compound **1**.

To obtain the concrete parameters for time dependence, the residual enzyme activities were measured at various inhibitor concentrations and incubation times (Figure 5B). The progress curves were fit to mathematical equations eqs 5−8 to determine $v_i$, $v_s$, and $k_{obs}$. Figure 5C shows the relationship between $k_{obs}$ and inhibitor concentration. This linear plot indicated that inhibitor **1** has the characteristic of a slow binding mode. The resulting kinetic parameters were $K_I^{app}$ = 0.064103 $\mu$M, $k_3$ = 0.2262 $\mu M^{-1}$ $min^{-1}$, and $k_4$ = 0.0145 $min^{-1}$, as determined through mathematical eqs 5−8.

**2.4.. Binding Affinities of Compounds to PTP1B.** The binding affinities of the selected inhibitors to the PTP1B enzyme were measured to explain the relationship between inhibitory potencies and binding affinities. The binding affinity was screened by a fluorescence quenching method. An interaction of enzymes with inhibitors leads to the intrinsic fluorescence (FS) of enzyme quench as a function of inhibitor concentrations. The PTP1B enzyme comprises a substantial number of intrinsic fluorescence residues consisting of 19 phenylalanines, 13 tyrosines, and 18 tryptophans.[31] Under our measurement settings, there was no discernible emission from any assay mixture (including the inhibitor). Figure 6 displayed the fluorescence emission spectra of the PTP1B enzyme from inhibitors (**1**−**3**) at different concentrations ranging from 0 to 25 $\mu$M. The FS reduction tendencies had a considerable relation with inhibitory potencies. As shown in Figure 6A, inhibitor **1** ($IC_{50}$ = 0.17 $\mu$M) showed a distinctive FS reduction pattern in comparison with that of inhibitor **3** ($IC_{50}$ = 17.79 $\mu$M). A similar FS reduction pattern was observed between inhibitors **2** and **3** (Figure 6B,C). The binding affinity constant ($K_{SV}$) was calculated by using the Stern−Volmer equation (Table 3). The $K_{SV}$ values were ranked in the order of inhibitory potencies (Figure 6D) as follows: compound **1** ($IC_{50}$ = 0.17 $\mu$M, $K_{SV}$ = 0.4375 × $10^5$ L·$mol^{-1}$) > **2** ($IC_{50}$ = 2.24 $\mu$M, $K_{SV}$ = 0.0304 × $10^5$ L·$mol^{-1}$) > **3** ($IC_{50}$ = 17.79 $\mu$M, $K_{SV}$ = 0.0006 × $10^5$ L·$mol^{-1}$. The fluorescence emission spectra of PTP1B at different concentrations (0, 1.6, 3.2, 6.2,

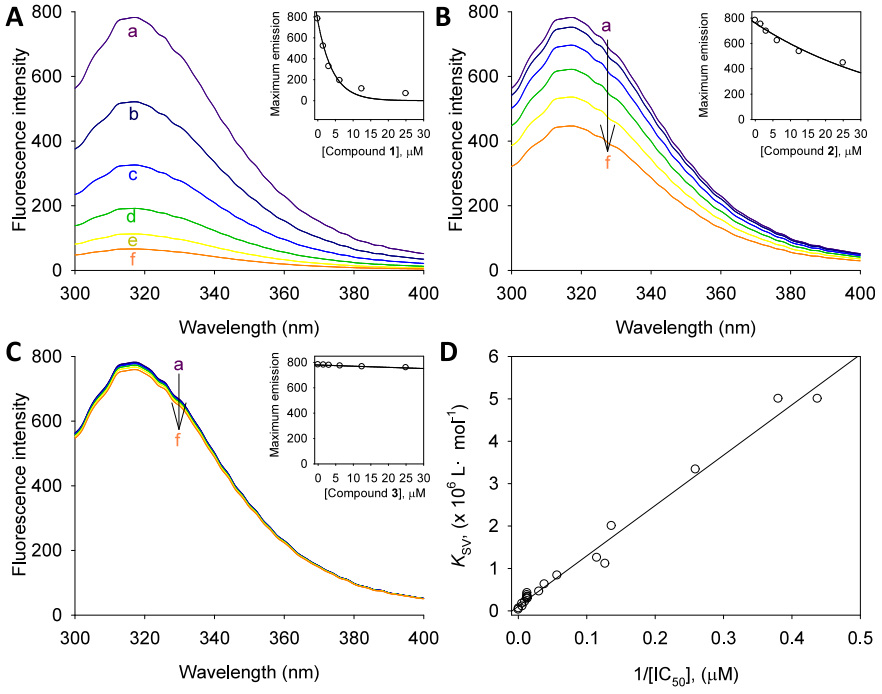


**Figure 6.** Fluorescence emission spectra of PTP1B at different concentrations (0, 1.6, 3.2, 6.2, 12.5, and 25 $\mu$M) of compounds (A) **1**, (B) **2**, (C) **3** (inset). Normalized intensities of fluorescence for PTP1B are shown. (D) The correlation between half-maximal PTP1B inhibitory concentration ($IC_{50}$s) values and Stern−Volmer constants ($K_{sv}$) of compounds **1**−**13**.



https://doi.org/10.1021/acsomega.3c07471
ACS Omega 2024, 9, 9053−9062

Table 3. Fluorescence Quenching Effect of Compounds 1−13 on PTP1B

| compounds | $K_{SV}$ ($\times 10^5$ L·mol$^{-1}$) | $R^a$ | $K_A$ ($\times 10^5$ L·mol$^{-1}$) | $n$ | $R^b$ |
|---|---|---|---|---|---|
| **1** | 0.4375 | 0.99 | 0.360 | 1.09 | 0.98 |
| **2** | 0.0304 | 0.98 | 0.027 | 1.16 | 0.97 |
| **3** | 0.0006 | 0.96 | 0.001 | 0.95 | 0.96 |
| **4** | 0.0135 | 0.97 | 0.016 | 0.99 | 0.96 |
| **5** | 0.0132 | 0.97 | 0.009 | 1.20 | 0.93 |
| **6** | 0.0002 | 0.84 | 0.001 | 0.79 | 0.98 |
| **7** | 0.0569 | 0.92 | 0.138 | 0.93 | 0.98 |
| **8** | 0.0056 | 0.87 | 0.013 | 1.02 | 0.97 |
| **9** | 0.1151 | 0.99 | 0.071 | 1.17 | 0.98 |
| **10** | 0.0124 | 0.98 | 0.012 | 1.06 | 0.96 |
| **11** | 0.0131 | 0.97 | 0.015 | 1.02 | 0.96 |
| **12** | 0.0098 | 0.97 | 0.007 | 1.18 | 0.93 |
| **13** | 0.3803 | 0.99 | 0.453 | 0.97 | 0.98 |

[a]$R$ is the correlation coefficient for the $K_{SV}$ values. [b]$R$ is the correlation coefficient for the $K_A$ values.

12.5, and 25 $\mu$M) of compounds **4**−**13** are shown in Figures S55−S56.

**2.5.. Predicting the Binding Modes between the New Compounds and the PTP1B by Molecular Docking Study.** To investigate the proper binding modes of compounds **1**, **2**, and **5** with PTP1B, the molecular docking (MD) method was employed. MD is one of the superior methods that predicts the binding modes of a given small molecule at the protein active site.[32] Prior toMD calculations, we collected 3D protein structure information and performed structural preparation for use in the study. Interestingly, it has been known that PTP1B has two binding sites, the catalytic site and the allosteric site. In this study, based on the experimental observations, compounds **1** and **2** were docked into the catalytic pocket only since both compounds were classified as competitive inhibitors. However, compound **5**, known as noncompetitive inhibitor was docked into both catalytic and allosteric sites for comparison purposes. The MD results at the catalytic site showed that the GOLD docking scores of compounds **1**, **2**, and **5** were 44.98, 44.93, and 44.3 respectively, and the docking score of compound **5** at the allosteric site was 54.65. In the final step, in order to obtain more refined binding modes from the docking results, the docked complexes between the compounds and proteins were energy-minimized using DS.

**2.6.. Comparison of the Binding Modes of Compounds 1 and 2 at the Catalytic Binding Sites.** The binding modes and molecular interactions of compounds **1** and **2**, known as competitive inhibitors, at the catalytic site were investigated using the molecular modeling study (Figure 7). The docking results showed that compound **1** had one conventional hydrogen bond with Asp48 and one carbon hydrogen bond with Gln262, including one $\pi$-cation interactions with Lys120, one $\pi-\pi$ stacked interaction with Tyr46, and two $\pi$-alkyl interaction with Tyr46 and Ala217. Several other residues also interacted with compound **1** by van der Waals interactions anchoring the compound to the binding pocket (Figure 7C). Compound **2** formed had two conventional hydrogen bonds with Asp48 and Gln262 and one $\pi-\pi$ stacked interaction with Tyr46 and two $\pi$-alkyl interactions with Tyr46, Lys120, and Ala217. Several other residues also interacted with compound **2** by van der Waals interactions

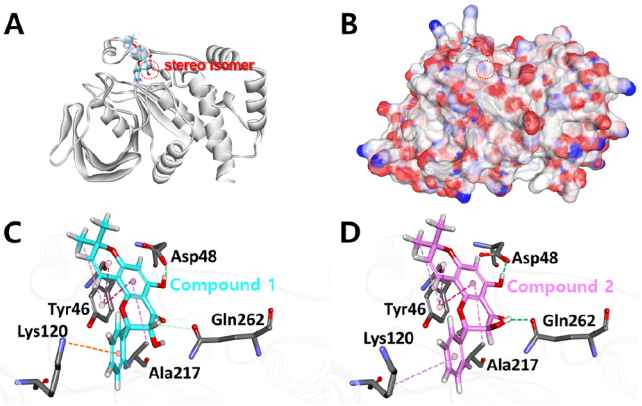


**Figure 7.** Comparison of the predicted binding modes of compounds **1** and **2** at the catalytic binding sites. (A) The homology model structure and (B) electrostatic surface model of PTP1B and compound **1** at the catalytic site. Compounds (C) **1** and (D) **2** ball-and-stick model to show clear intermolecular interact. Conventional hydrogen bonds, carbon−hydrogen bonds, $\pi$-cation interactions, $\pi-\pi$ stacked interactions, and $\pi$-alkyl interactions are colored green, bright green, orange, magenta, and pink, respectively.

anchoring the compound to the binding pocket (Figure 7D). The main difference between compound **1** and **2** is the stereo isomer relationship for the −OH group in the main skeleton. The overall binding patterns of both compounds are very similar (Figure 7C,D). The only difference is the terminal atom or group that interacts with Gln262 of PTP1B. In compound **1**, the hydrogen atom (H-3) in the main skeleton ring forms a carbon hydrogen bond with Gln262. However, in compound **2**, the hydrogen atom in the −OH group forms a conventional hydrogen bond with Gln262.

Overall protein−ligand binding morphology of the docking structures of compounds **1** and **2** with PTP1B was shown in a ball-and-stick model (A) and an electrostatic surface model to show the binding pocket geometry of the protein (B). And the detailed interaction networks for the bonding modes were visualized in panels C and D. All interactions are shown as dashed lines. Conventional hydrogen bonds, carbon−hydrogen bonds, $\pi$-cation interactions, $\pi-\pi$ stacked interaction, and $\pi$-alkyl interactions are shown in green, bright green, orange, magenta, and pink, respectively.

**2.7.. Binding Mode Analysis of the Compound 5 in the Active and Allosteric Sites.** In order to find out the reason why compound **5** is classified as a noncompetitive, the binding mode and molecular interaction of compound **5** were investigated and compared at the catalytic and allosteric sites (Figure 8). The results showed that compound **5** at the catalytic site had three alkyl interactions with Arg45, Tyr46, and Lys120, two $\pi$-alkyl interactions with Cys215 and Ala217, and one $\pi-\pi$ T-shaped interaction with Tyr46. Several other residues also interacted with compound **5** by van der Waals interactions anchoring the compound to the binding pocket (Figure 8C). On the other hand, compound **5** in the allosteric site had one conventional hydrogen bond with Asn193, including two $\pi-\pi$ stacked interactions with Phe196 and Phe280 and three alkyl interactions with Ala189, Leu192, and Pro188. Several other residues also interacted with compound **5** by van der Waals interactions anchoring the compound to the binding pocket (Figure 8D).

Docking scores of compound **5** at the catalytic and allosteric sites were 44.3 and 54.65, respectively. Interestingly, our


https://doi.org/10.1021/acsomega.3c07471
ACS Omega 2024, 9, 9053−9062

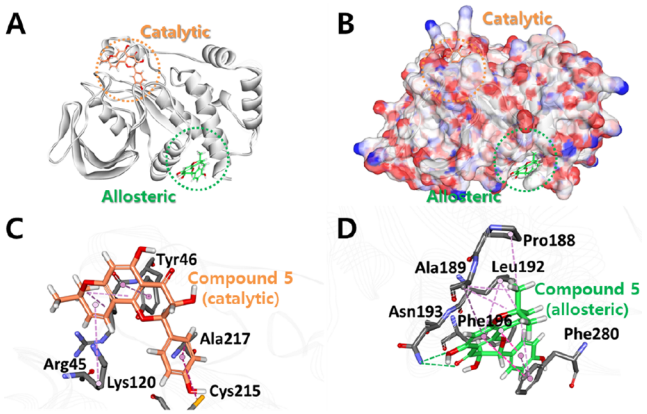


**Figure 8.** Comparison of the predicted binding modes of compound **5** at the catalytic and allosteric binding sites. (A) The homology model structure and (B) electrostatic surface model of the PTP1B and compound **5** at catalytic and allosteric sites. The ball-and-stick model of compound **5** shows clear intermolecular interaction at the (C) catalytic and (D) allosteric sites.

docking result suggests that compound **5** is more stable at the allosteric pocket. This result is very compatible with our experimental findings.

Overall, protein−ligand binding morphology of the docking structures of compound **5** in the catalytic and allosteric sites of PTP1B is shown in a ball-and-stick model (Figure 8A) and electrostatic surface model to show the binding pocket geometry of the protein (Figure 8B). And the detailed interaction networks for the bonding modes are visualized in panels C and D. All interactions are shown as dashed lines. Conventional hydrogen bonds, carbon−hydrogen bonds, $\pi$-cation interactions, $\pi-\pi$ stacked interaction, and $\pi$-alkyl interactions are shown in green, bright green, orange, magenta, and pink, respectively.

## 3.. CONCLUSION

This study explored PTP1B inhibitory metabolites from the leaves of *Artocarpus elasticus*. The responsible metabolites for PTP1B ($IC_{50}$ = 0.17−35.41 $\mu$M) were identified as eight dihydroflavonols (**1**−**6**, **11**, **12**) and five flavones (**7**−**10**, **13**). Inhibitory potency and behavior were significantly affected by chemical skeleton and functionality. For example, all dihydroflavonols (**1**−**4**) with a simple phenyl group at the B-ring showed competitive inhibition. The new compounds were diastereomers of each other, which were confirmed by NOESY experiments. The slow binding characteristics were observed on the most active inhibitor, **1** ($IC_{50}$ = 0.17 $\mu$M). Defying general expectations, flavonol glycosides (**11** and **13**) showed significant inhibition with $IC_{50}$s of 2.39 and 0.22 $\mu$M, respectively. The binding affinities to enzymes had a high correlation with inhibitory potencies. The specific interaction between inhibitors and enzyme was proposed by molecular docking experiments. Overall, this work represents the most intensive metabolite and biological study, which could contribute to nutraceutical applications of *A. elasticus* leaves. It also provides a lead structure for PTP1B inhibition with a very reasonable scientific story.

## 4.. MATERIALS AND METHODS

**4.1.. Chemicals and Materials.** Used chemicals were of analytical grade and were bought from Thermo Fisher Scientific (Waltham, Massachusetts, USA). Octadecylsilanized (ODS) silica gel (YMC Ltd., Japan), Sephadex LH-20 (Amersham Pharmacia Biotech, Sweden), and MCI GEL CHP20P (Sigma-Aldrich Korea, Seoul, South Korea) were used as packing materials for column chromatography. Recycling HPLC (LC-Forte/R100, YMC Co., LTD, Kyoto, Japan) system arranged with a UV detector was used for the isolation and purification of compounds. NMR spectra of the purified compounds were conducted on a Bruker (AM 300, 500 MHz) and JEOL JMS-700 (JEOL Ltd., Akishima, Japan) was used for the MS. The CD spectra were recorded on a Jasco J-815 (Japan) CD spectrophotometer. The enzyme inhibition assays were evaluated on a SpectraMaxM3Multi-Mode Microplate Reader (Molecular device, USA).

**4.2.. Plant Material.** *Artocarpus elasticus* leaves were collected in December 2013 in Malaysia by Associate Professor Dr Mohd Azlan Nafiah. The voucher for the specimen (TM1016) was provided by Universiti Pendidikan Sultan Idris, Malaysia.

**4.3.. Extraction and Isolation.** The air-dried leaves (0.8 kg) of *A. elasticus* were extracted in methanol (10 L) three times at 20−23 °C with yielding extract of 53 g. Then methanol extract was first suspended in water and fractionated into 28 g of the chloroform extract. The obtained chloroform fraction was then passed from column chromatography on MCI GEL CHP20P (30.0 × 5.0 cm, 75−150 $\mu$m, 0.5 kg) and with a gradient flow of water/methanol (9:1 to 0:1, v/v) resulted in 17 subfractions (AC1−17). ODS (25.0 × 3.0 cm, S-10 $\mu$m, 12 nm) was then used for fractions AC2-5 (5 g) with solvent using MeOH from 0 to 100% in water that give 70 subfractions (ACX1-70). Recycled HPLC (25.0 × 1.5 cm, S-5 $\mu$m, 12 nm) was used for ACX20-40 yielding compounds **6** (16 mg), **7** (11 mg), **8** (10 mg), and **9** (10.5 mg), and the fractions ACX50-70 were also passed through similar way, which resulted in compounds **3** (102 mg), **4** (11 mg), **5** (17 mg), **10** (7 mg), and **11** (15 mg). Further, AC6-8 (4.8 g) were passed through MPLC (250 × 30.0 mm, S-10 $\mu$m, 12 nm, YMC) eluting with a gradual increase of MeOH from 0 to 100% in water resulting in ACY1-50 subfractions, which when eluted with 100% methanol in Sephadex LH-20 and recycled HPLC (25.0 × 1.5 cm, S-5 $\mu$m, 12 nm) yielded compounds **1** (15 mg) and **2** (13 mg). AC10-15 resulted in compounds **12** (25 mg) and **13** (20 mg), by subjecting to repeated recycled HPLC (25.0 × 3.0 mm, S-5 $\mu$m, 12 nm).

*4.3.1.. Compound 3.* (Artoscortonol B): Yellowish crystals; ESIMS $m/z$ 355 $[M + H]^+$; HRESIMS $m/z$ 355.1545 $[M + H]^+$ (calcd for $C_{21}H_{22}O_5$ 354.1467). $^1$H NMR (500 MHz, methanol−$d_4$) $\delta$ 1.48 (3H, s, H-4″), 1.60 (3H, s, H-5″), 3.16 (2H, m, H-1″), 3.82 (3H, s, OMe), 4.36 (1H, d, $J$ = 11.7 Hz, H-3), 4.98 (1H, d, $J$ = 11.75 Hz, H-2), 5.11 (1H, t, $J$ = 14.45 Hz, H-2″), 6.15 (1H, s, H-6), 7.39 (3H, m, H-3′, 4′, 5′), 7.53 (2H, m, H-2′, 6′).

*4.3.2.. Compound 4.* (Glepidotin B): Yellow powder; ESIMS $m/z$ 341 $[M + H]^+$; HRESIMS $m/z$ 341.1389 $[M + H]^+$ (calcd for $C_{20}H_{20}O_5$ 340.1311). $^1$H NMR (500 MHz, acetone−$d_6$) $\delta$ 1.54 (3H, s, H-5″), 1.60 (3H, s, H-4″), 3.18 (2H, m, H-1″), 4.61 (1H, dd, $J$ = 11.47, H-3), 5.15 (1H, brs, Hz, H-2″), 5.17 (1H, brs, H-2), 6.09 (1H, s, H-6), 7.41 (3H, m, H-3′, 4′, 5′), 7.61 (2H, m, H-2′, 6′).

*4.3.3.. Compound 5.* (Yukovanol): White powder; ESIMS $m/z$ 355 $[M + H]^+$; HRESIMS $m/z$ 355.1182 $[M + H]^+$ (calcd for $C_{20}H_{18}O_6$ 354.1103). $^1$H NMR (500 MHz, acetone−$d_6$) $\delta$ 1.41 (3H, s, H-5″), 1.43 (3H, s, H-4″), 4.67 (1H, d, $J$ = 11.5


https://doi.org/10.1021/acsomega.3c07471
ACS Omega 2024, 9, 9053−9062

Hz, H-3), 5.14 (1H, $J$ = 11.6, H-2), 5.58 (1H, d, $J$ = 10.1 Hz, H-2″), 5.92 (1H, s, H-6), 6.42 (1H, d, $J$ = 10.1 Hz, H-1″), 6.89 (1H, d, $J$ = 8.5 Hz, H-3′, 5′), 7.4 (2H, d, $J$ = 8.5 Hz, H-2′, 6′).

*4.3.4.. Compound 6.* (Dihydrokaempferol): yellow needles; EIMS, $m/z$ 288 $[M]^+$; HREIMS, $m/z$ 288.0632 $[M + H]^+$ (calcd for $C_{15}H_{12}O_6$ 288.0634); $^1$H NMR (500 MHz, methanol−$d_4$) $\delta$ 4.53 (1H, d, $J$ = 11.6 Hz, H-3), 4.96 (1H, d, $J$ = 11.6 Hz, H-2), 5.88 (1H, s, H-6), 5.92 (1H, s, H-8), 6.83 (2H, d, $J$ = 8.6 Hz, H-3′, H-5′), 7.34 (2H, d, $J$ = 8.55 Hz, H-2′, H-6′).

*4.3.5.. Compound 7.* (Atalantoflavone): Yellow Powder; ESIMS $m/z$ 337 $[M + H]^+$; HRESIMS $m/z$ 337.1079 $[M + H]^+$ (calcd for $C_{20}H_{16}O_5$ 336.0998). $^1$H NMR (500 MHz, methanol−$d_4$) $\delta$ 1.47 (6H, s, H-4″, 5″), 5.70 (1H, d, $J$ = 10.05 Hz, H-2″), 6.47 (1H, s, H-6), 6.61 (1H, s, H-3), 6.66 (1H, d, $J$ = 10.1 Hz, H-1″), 6.91 (2H, d, $J$ = 8.8 Hz, H-3′, 5′), 7.84 (2H, d, $J$ = 8.85 Hz, H-2′, 6′).

*4.3.6.. Compound 8.* (Apigenin): Yellow needles; EIMS, $m/z$ 271 $[M + H]^+$; HRESIMS, $m/z$ 271.0606 $[M + H]^+$ (calcd for $C_{15}H_{11}O_5$ 270.0528); $^1$H NMR (500 MHz, DMSO−$d_6$) $\delta$ 6.18 (1H, d, $J$ = 2.0 Hz, H-6), 6.47 (1H, d, $J$ = 2.0 Hz, H-8), 6.53 (1H, s, H-3), 6.90 (2H, d, $J$ = 8.8 Hz, H-3′, 5′), 7.91 (2H, d, $J$ = 8.8 Hz, H-2′, 6′), 12.95 (1H, s, 5-OH).

*4.3.7.. Compound 9.* (2′-Hydroxyatalantoflavone): Reddish gummy solid; FABMS $m/z$ 353 $[M + H]^+$; HRFABMS $m/z$ 353.1006 $[M + H]^+$ (calcd for $C_{20}H_{17}O_6$ 352.0947). $^1$H NMR (500 MHz, acetone−$d_6$) $\delta$ 1.40 (3H, s, H-5″), 1.42 (3H, s, H-4″), 5.69 (1H, d, $J$ = 8 Hz, H-2″), 6.40 (1H, s, H-6), 6.51 (1H, s, H-5′), 6.56 (1H, s, H-3′), 6.63 (1H, d, $J$ = 8 Hz, H-1″), 7.05 (1H, s, H-3), 7.8 (1H, s, H-6′).

*4.3.8.. Compound 10.* (Norartocarpetin): Yellowish white amorphous powder; EIMS, $m/z$ 286 $[M]^+$; HREIMS, $m/z$ 286.0472 $[M + H]^+$ (calcd for $C_{15}H_{10}O_6$ 286.0477); $^1$H NMR (500 MHz, acetone-$d_6$) $\delta$ 6.23 (1H, d, $J$ = 2.1 Hz, H-6), 6.49 (1H, d, $J$ = 2.1 Hz, H-5′), 6.55 (1H, dd, $J$ = 8.75 Hz, H-3′), 6.61 (1H, d, $J$ = 2.3 Hz, H-8), 7.07 (1H, s, H-3), 7.83 (1H, d, $J$ = 8.75 Hz, H-6′).

*4.3.9.. Compound 11.* (Engeletin): White needles; FABMS $m/z$ 435 $[M + H]^+$; HRFABMS $m/z$ 435.1300 $[M]^+$ (calcd for $C_{21}H_{23}O_{10}$ 434.1213). $^1$H NMR (500 MHz, acetone−$d_6$) $\delta$ 1.15 (3H, s, H-6″), 3.37 (1H, s, H-5″), 3.59 (1H, s, H-4″), 3.71 (1H, s, H-3″), 4.01 (1H, s, H-1″), 4.25 (1H, s, H-2″), 4.67 (1H, d, $J$ = 10.8 Hz, H-3), 5.19 (1H, d, $J$ = 10.8 Hz, H-2), 5.94 (1H, d, $J$ = 2.05 Hz, H-8), 5.98 (1H, d, $J$ = 1.5 Hz, H-6), 6.89 (1H, d, $J$ = 8.5 Hz, H-5′), 6.91 (1H, d, $J$ = 8.5 Hz, H-3′), 7.40 (1H, d, $J$ = 8.5 Hz, H-6′), 7.41 (1H, d, $J$ = 8.5 Hz, H-2′).

*4.3.10.. Compound 12.* (Isoengeletin): White powder; FABMS $m/z$ 435 $[M + H]^+$; HRFABMS $m/z$ 435.1300 $[M]^+$ (calcd for $C_{21}H_{23}O_{10}$ 434.1213). $^1$H NMR (500 MHz, acetone−$d_6$) $\delta$ 0.78 (3H, d, $J$ = 6.15 Hz, H-6″), 3.02 (1H, s, H-5″), 3.15 (1H, s, H-4″), 3.44 (1H, s, H-3″), 4.16 (1H, d, $J$ = 2.46 Hz, H-2″), 4.49 (1H, dd, $J$ = 4.49, 14.6 Hz, H-3), 4.74 (1H, s, H-1″), 4.79 (1H, dd, $J$ = 4.29, 14.6 Hz, H-2), 5.92 (1H, d, $J$ = 2.1 Hz, H-8), 5.95 (1H, d, $J$ = Hz, H-6), 6.74 (1H, d, $J$ = 2.1 Hz, H-5′), 6.77 (1H, d, $J$ = 8.61 Hz, H-3′), 7.24 (1H, d, $J$ = 8.61 Hz, H-6′), 7.27 (1H, d, $J$ = Hz, H-2′).

*4.3.11.. Compound 13.* (Apigenin-7-*O*-$\beta$-D-glucopyranoside): Pale yellow amorphous powder, HRESIMS: $m/z$ 433.1160 $[M + H]^+$ (calcd. for $C_{21}H_{21}O_{10}$ 432.1056). $^1$H NMR (500 MHz, DMSO-$d_6$) $\delta$ 3.26−3.36 (4H, m, H-2″ to H-5″), 3.45 (1H, m, H-6b″), 3.73 (1H, d, $J$ = 10.5 Hz, H-6a″) 5.06 (1H, d, $J$ = 7.4 Hz, H-1″), 6.44 (1H, d, $J$ = 2.0 Hz, H-6), 6.83 (1H, br s, H-8), 6.85 (1H, s, H-3), 6.93 (2H, d, $J$ = 8.7 Hz, H-3′, 5′), 7.95 (2H, d, $J$ = 8.6 Hz, H-2′, 6′).

**4.4.. PTP1B Inhibitory Assay.** The inhibitory potential of compounds (**1**−**13**) was evaluated against PTP1B according to the previously published literature.[29] The human recombinant PTP1B enzyme (EC 3.1.3.48) was purchased from Enzo Life Sciences Inc. (Farmingdale, NY, USA). Compounds, including positive controls, were solubilized in DMSO before being diluted to the needed concentration. The required buffer was Tris-HCl (pH 7.5), which was prepared by taking 25 mM Tris, 1 mM EDTA, 2 mM 2-mercaptoethanol, and 1 mM dithiothreitol. The pH was attained by using HCl. Further, 130 $\mu$L buffer, 10 $\mu$L of the sample, 40 $\mu$L of *p*-nitrophenyl phosphate (*p*NPP, 0.8 mM treated concentration) as a substrate, and 20 $\mu$L of the enzyme (1 $\mu$g/mL treated concentration) were taken in 96-well plate, and the reaction of succeeding hydrolysis of *p*NPP was observed for 30 min at 405 nm and 37 °C. After 10 min of incubation, the values were noted. Half maximal inhibitory concentration ($IC_{50}$) was calculated from the conversion of eq 1.

$$\text{Activity}(\%) = 100[1/(1 + ([I]/IC_{50}))] \quad (1)$$

**4.5.. Enzyme Kinetic Assay.** The detailed kinetic study of PTP1B was evaluated using Lineweaver−Burk and Dixon plots. The kinetic parameters related to the inhibition mechanism were derived from various inhibitor and substrate concentrations by applying steady-state rates. These two inhibition constants—$K_I$ for free enzyme and $K_{IS}$ for the enzyme−substrate complex—were derived from secondary plots of the slopes of the straight lines or vertical intercept ($1/V_{max}$) vs inhibitor concentration, respectively. $K_I$ and $K_{IS}$ were derived by applying eqs 2−4.[29,33]

$$\frac{1}{V} = \frac{K_m}{V_{max}}\left(1 + \frac{[I]}{K_I}\right)\frac{1}{[S]} + \frac{1}{V_{max}} \quad (2)$$

$$\text{Slope} = \frac{K_m}{K_I V_{max}}[I] + \frac{K_m}{V_{max}} \quad (3)$$

$$\text{Intercept} = \frac{K_m}{K_{IS} V_{max}}[I] + \frac{1}{V_{max}} \quad (4)$$

**4.6.. Time-Dependent Assays and Progress Curves.** To learn more about PTP1B's kinetic and time-dependent inhibitory parameters, using actual substrate concentration, the progress curves were obtained at different concentrations of inhibitors. Any lag (around 10 min) period was excluded while determining progress curves. The data that give the specific parameters for each curve; $v_i$ (initial velocity), $v_s$ (steady-state velocity), $k_{obs}$ (apparent first-order rate constant for the transition from $v_i$ to $v_s$), $A$ (absorbance at 405 nm), and $K_i^{app}$ (apparent $K_i$) were calculated by using Sigma plot (SPCC Inc., Chicago, IL) conforming to the following eqs 5)−8.[29,34]

$$\frac{[P]^t}{[E]} = v_i t + \frac{(v_i + v_s)}{k_{obs}}(1 - e^{-k_{obs}}) \quad (5)$$

$$\frac{v}{v_0} = e^{-k_{obs}} \quad (6)$$

$$k_{obs} = k_4 + \frac{k_4 + [I]}{k_i^{appt}} \quad (7)$$



https://doi.org/10.1021/acsomega.3c07471
ACS Omega 2024, 9, 9053−9062

$$K_i = \frac{k_4}{k_3} \quad (8)$$

**4.7.. Fluorescence Spectra Measurement for Binding Affinity to PTP1B.** The binding affinity of PTP1B was measured by taking 180 μL of buffer with 10 μL of the enzyme (concentration was similar to the previous assays) in 96-well black immuno plates and then 10 μL of different concentrations of the inhibitor was added. The fluorescence emission spectra were recorded in a spectrometer with 300−400 nm, and emission and excitation were 250 nm with slits of 2 nm. The Stern−Volmer constant ($K_{SV}$), binding constant ($K_A$), and number of binding sites ($n$), which are all quenching parameters, were calculated using eqs 9 and 10:[35]

$$F_0 - F = 1 + K_{SV}[Q]_f \quad (9)$$

$$\log \frac{F_0 - F}{F} = \log K_A + n\log [Q]_f \quad (10)$$

where $F_0$ and $F$ are the fluorescence intensities in the absence and presence of a quencher. $[Q]_f$ is the concentration of compounds.

**4.8.. Molecular Docking Study.** The crystal structure of PTP1B (PDB ID: 1T49) with a resolution of 1.9 Å was obtained from RCSB Protein Data Bank (www.rcsb.org).[36] Subsequently, the protein was prepared by enabling the *Clean Protein* tool accessible in Discovery Studio (DS) v2019. The water molecules and heteroatoms were removed, and the protein was minimized employing *Minimize and Refine Protein* module available in the DS. For the molecular docking (MD) study, the three-dimensional (3D) structures of three inhibitors, compounds **1**, **2**, and **5** were prepared using *sketching tool* (Marvin sketch JS) and the structures were optimized employing the *Avogadro* program. For exploring the binding modes of the three inhibitors withPTP1B, GOLD Version 5.2.2 (Cambridge Crystallo-graphic Data Center, UK) that used genetic algorithms was employed.[37] Correspondingly, the docking site was defined within 10 Å around the catalytic and allosteric sites with references to the docking studies as reported previously.[38,39] During the docking computations, each ligand was allowed to generate 10 conformations, while retaining the other parameters as default. The best binding modes of compounds were selected based on the highest GOLD fitness score.

## ■ ASSOCIATED CONTENT

### Supporting Information

The Supporting Information is available free of charge at https://pubs.acs.org/doi/10.1021/acsomega.3c07471.

Supporting Information are includes$^{13}$C NMR data of compounds **1**−**13** (page S2), 1D, 2D NMR, and HREIMS data of compounds **1**−**13** (page S4), CD spectra of compounds **1** and **2** (page S32), Lineweaver−Burk and Dixon plots for PTP1B inhibition compounds **2**−**4**, **6**−**12** (page S33), fluorescence quenching data for PTP1B of compounds **4**−**13** (page S37), mass characterization of compounds isolated from the leaves of *A. elasticus* (page S39) (PDF)

## ■ AUTHOR INFORMATION


### Corresponding Author

**Ki Hun Park** − *Division of Applied Life Science (BK21 Four), IALS, Gyeongsang National University, Jinju 52828, Republic of Korea;* orcid.org/0000-0003-4467-2709; Phone: +82-55-772-1965; Email: khpark@gnu.ac.kr; Fax: +82-55-772-1969

### Authors

**Abdul Bari Shah** − *Division of Applied Life Science (BK21 Four), IALS, Gyeongsang National University, Jinju 52828, Republic of Korea;* orcid.org/0000-0002-2918-7556

**Aizhamal Baiseitova** − *Division of Applied Life Science (BK21 Four), IALS, Gyeongsang National University, Jinju 52828, Republic of Korea*

**Gihwan Lee** − *Division of Applied Life Science (BK21 Four), ABC-RLRC, PMBBRC, Gyeongsang National University, Jinju 52828, Korea*

**Jeong Ho Kim** − *Division of Applied Life Science (BK21 Four), IALS, Gyeongsang National University, Jinju 52828, Republic of Korea*

Complete contact information is available at: https://pubs.acs.org/10.1021/acsomega.3c07471


### Author Contributions

B.S.: Conceptualization, Investigation, Data Curation, Writing − Original Draft, Visualization. A.B.: Conceptualization, Investigation, Validation, Supervision, Writing − Review & Editing. G.L.: Investigation, Software, Conceptualization, Writing − Original Draft. J.H.K.: Investigation, Formal analysis. $K_i$. H.P.: Conceptualization, Resources, Writing − Original Draft, Writing − Review & Editing, Supervision, Project administration, Funding acquisition.

### Notes

The authors declare no competing financial interest.

## ■ ACKNOWLEDGMENTS

The research was supported by Basic Science Research Program (NRF-2022R1A2C1091270) of the National Research Foundation (NRF) funded by the Ministry of Science and ICT, the National Research Foundation (NRF) grant (No. 2015R1A6A1A03031413) by the Ministry of Education, Republic of Korea. The BK21 plus program supported scholarships for all students. The researchers received no external funding.

## ■ REFERENCES

(1) Johnson, T. O.; Ermolieff, J.; Jirousek, M. R. Protein Tyrosine Phosphatase 1B Inhibitors for Diabetes. *Nat. Rev. Drug Discovery* **2002**, *1* (9), 696−709.

(2) Rath, P.; Ranjan, A.; Ghosh, A.; Chauhan, A.; Gurnani, M.; Tuli, H. S.; Habeeballah, H.; Alkhanani, M. F.; Haque, S.; Dhama, K.; Verma, N. K.; Jindal, T. Potential Therapeutic Target Protein Tyrosine Phosphatase-1B for Modulation of Insulin Resistance with Polyphenols and Its Quantitative Structure−Activity Relationship. *Molecules* **2022**, *27* (7), 2212.

(3) Xue, B.; Kim, Y.-B.; Lee, A.; Toschi, E.; Bonner-Weir, S.; Kahn, C. R.; Neel, B. G.; Kahn, B. B. Protein-Tyrosine Phosphatase 1B Deficiency Reduces Insulin Resistance and the Diabetic Phenotype in Mice with Polygenic Insulin Resistance. *J. Biol. Chem.* **2007**, *282* (33), 23829−23840.

(4) Elchebly, M.; Payette, P.; Michaliszyn, E.; Cromlish, W.; Collins, S.; Loy, A. L.; Normandin, D.; Cheng, A.; Himms-Hagen, J.; Chan, C. C.; Ramachandran, C.; Gresser, M. J.; Tremblay, M. L.; Kennedy, B.

P. Increased Insulin Sensitivity and Obesity Resistance in Mice Lacking the Protein Tyrosine Phosphatase-1B Gene. *Science* **1999**, *283* (5407), 1544−1548.
(5) Norris, K.; Norris, F.; Kono, D. H.; Vestergaard, H.; Pedersen, O.; Theofilopoulos, A. N.; Møller, N. P. H. Expression of Protein-Tyrosine Phosphatases in the Major Insulin Target Tissues. *FEBS Lett.* **1997**, *415* (3), 243−248.
(6) Cho, H. Chapter Seventeen - Protein Tyrosine Phosphatase 1B (PTP1B) and Obesity. In *Vitamins & Hormones*, Litwack, G., Ed.; Obesity; Academic Press, 2013; Vol. *91*, pp 405424. .
(7) Daus, M.; Chaithada, P.; Phongpaichit, S.; Watanapokasin, R.; Carroll, A. R.; Mahabusarakam, W. New Prenylated Dihydrochalcones from the Leaves of *Artocarpus Elasticus*. *Phytochem. Lett.* **2017**, *19*, 226−230.
(8) Ban, Y. J.; Baiseitova, A.; Nafiah, M. A.; Kim, J. Y.; Park, K. H. Human Neutrophil Elastase Inhibitory Dihydrobenzoxanthones and Alkylated Flavones from the *Artocarpus Elasticus* Root Barks. *Appl. Biol. Chem.* **2020**, *63* (1), 63.
(9) Baiseitova, A.; Shah, A. B.; Khan, A. M.; Idrees, M.; Kim, J. H.; Lee, Y. H.; Kong, I.-K.; Park, K. H. Antioxidant Potentials of Furanodihydrobenzoxanthones from *Artocarpus Elasticus* and Their Protection against oxLDL Induced Injury in SH-SY5Y Cells. *Biomed. Pharmacother.* **2023**, *165*, 115278.
(10) Baiseitova, A.; Lee, G.; Shah, A. B.; Yoon, S.; Kim, J. H.; Lee, Y. H.; Park, K. H. New Dihydrobenzoxanthone Derivatives with Bacterial Neuraminidase Inhibitory Activity Isolated from *Artocarpus Elasticus*. *Bioorg. Chem.* **2022**, *127*, 105978.
(11) Jenis, J.; Baiseitova, A.; Yoon, S. H.; Park, C.; Kim, J. Y.; Li, Z. P.; Lee, K. W.; Park, K. H. Competitive $\alpha$-Glucosidase Inhibitors, Dihydrobenzoxanthones, from the Barks of *Artocarpus Elasticus*. *J. Enzyme Inhib. Med. Chem.* **2019**, *34* (1), 1623−1632.
(12) Kijjoa, A.; Cidade, H. M.; Pinto, M. M. M.; Gonzalez, M. J. G.; Anantachoke, C.; Gedris, T. E.; Herz, W. Prenylflavonoids from *Artocarpus Elasticus*. *Phytochemistry* **1996**, *43* (3), 691−694.
(13) Lin, K.-W.; Liu, C.-H.; Tu, H.-Y.; Ko, H.-H.; Wei, B.-L. Antioxidant Prenylflavonoids from Artocarpus Communis and *Artocarpus Elasticus*. *Food Chem.* **2009**, *115* (2), 558−562.
(14) Ramli, F.; Rahmani, M.; Ismail, I. S.; Sukari, M. A.; Abd Rahman, M.; Zajmi, A.; Akim, A. M.; Hashim, N. M.; Go, R. A New Bioactive Secondary Metabolite from *Artocarpus Elasticus*. *Nat. Prod. Commun.* **2016**, *11* (8), 1103−1106.
(15) Ramli, F.; Rahmani, M.; Kassim, N. K.; Hashim, N. M.; Sukari, M. A.; Akim, A. M.; Go, R. New Diprenylated Dihyrochalcones from Leaves of *Artocarpus Elasticus*. *Phytochem. Lett.* **2013**, *6* (4), 582−585.
(16) Grosvenor, P. W.; Gothard, P. K.; McWilliam, N. C.; Supriono, A.; Gray, D. O. Medicinal Plants from Riau Province, Sumatra, Indonesia. Part 1: Uses. *J. Ethnopharmacol.* **1995**, *45* (2), 75−95.
(17) Lathiff, S.; Mariam, A.; Arriffin, N.; Jamil, S. P. Phytochemicals, Pharmacological and Ethnomedicinal Studies of *Artocarpus*: A Scoping Review. *Asian Pac. J. Trop. Biomed.* **2021**, *11* (11), 469.
(18) Jagtap, U. B.; Bapat, V. A. *Artocarpus*: A Review of Its Traditional Uses, Phytochemistry and Pharmacology. *J. Ethnopharmacol.* **2010**, *129* (2), 142−166.
(19) Mohd Arriffin, N.; Jamil, S.; Basar, N. Two New Dihydroflavonols from the Leaves of *Artocarpus Scortechinii* King. *Phytochem. Lett.* **2021**, *41*, 139−141.
(20) Manfredi, K. P.; Vallurupalli, V.; Demidova, M.; Kindscher, K.; Pannell, L. K. Isolation of an Anti-HIV Diprenylated Bibenzyl from *Glycyrrhiza Lepidota*. *Phytochemistry* **2001**, *58* (1), 153−157.
(21) Ito, C.; Sato, K.; Oka, T.; Inoue, M.; Ju-Ichi, M.; Omura, M.; Furukawa, H. Two Flavanones from Citrus Species. *Phytochemistry* **1989**, *28* (12), 3562−3564.
(22) Sasaki, H.; Kashiwada, Y.; Shibata, H.; Takaishi, Y. Prenylated Flavonoids from *Desmodium Caudatum* and Evaluation of Their Anti-MRSA Activity. *Phytochemistry* **2012**, *82*, 136−142.
(23) Banerji, A.; Luthria, D. L.; Prabhu, B. R. Prenylated Compounds from *Atalantia Racemosa*: Isolation and Synthesis of Two Pyranoflavones. *Phytochemistry* **1988**, *27* (11), 3637−3640.
(24) Kumar, K. S.; Sabu, V.; Sindhu, G.; Rauf, A. A.; Helen, A. I. Isolation, Identification and Characterization of Apigenin from *Justicia Gendarussa* and Its Anti-Inflammatory Activity. *Int. Immunopharmacol.* **2018**, *59*, 157−167.
(25) Ouete, J. L. N.; Sandjo, L. P.; Liermann, J. C.; Opatz, T.; Simo, I. K.; Ngadjui, B. T. A New Flavone From The Roots Of *Milicia Excelsa* (Moraceae). *Z. Naturforsch., C: J. Biosci.* **2014**, *68*, 7−8.
(26) Xu, J.; Li, X.; Zhang, P.; Li, Z.-L.; Wang, Y. Antiinflammatory Constituents from the Roots of Smilax Bockii Warb. *Arch. Pharm. Res.* **2005**, *28* (4), 395−399.
(27) Benavente-García, O.; Castillo, J.; Lorente, J.; Ortuño, A.; Del Rio, J. A. Antioxidant Activity of Phenolics Extracted from *Olea Europaea* L. Leaves. *Food Chem.* **2000**, *68* (4), 457−462.
(28) Prescott, A. G.; Stamford, N. P. J.; Wheeler, G.; Firmin, J. L. In Vitro Properties of a Recombinant Flavonol Synthase from *Arabidopsis Thaliana*. *Phytochemistry* **2002**, *60* (6), 589−593.
(29) Shah, A. B.; Yoon, S.; Kim, J. H.; Zhumanova, K.; Ban, Y. J.; Lee, K. W.; Park, K. H. Effectiveness of Cyclohexyl Functionality in Ugonins from *Helminthostachys Zeylanica* to PTP1B and $\alpha$-Glucosidase Inhibitions. *Int. J. Biol. Macromol.* **2020**, *165*, 1822−1831.
(30) Le, T. T.; Ha, M. T.; Cao, T. Q.; Kim, J. A.; Choi, J. S.; Min, B. S. 1,5-Anhydro-d-Glucitol Derivative and Galloylated Flavonoids Isolated from the Leaves of Acer Ginnala Maxim. as Dual Inhibitors of PTP1B and $\alpha$-Glucosidase Enzymes: In Vitro and in Silico Studies. *Phytochemistry* **2023**, *213*, 113769.
(31) Papadopoulou, A.; Green, R. J.; Frazier, R. A. Interaction of Flavonoids with Bovine Serum Albumin: A Fluorescence Quenching Study. *J. Agric. Food Chem.* **2005**, *53* (1), 158−163.
(32) Meng, X.-Y.; Zhang, H.-X.; Mezei, M.; Cui, M. Molecular Docking: A Powerful Approach for Structure-Based Drug Discovery. *Curr. Comput.-Aided Drug Des.* **2011**, *7* (2), 146−157.
(33) Baiseitova, A.; Ban, Y. J.; Kim, J. Y.; Lee, G.; Shah, A. B.; Kim, J. H.; Lee, Y. H.; Park, K. H. Soybean Phytochemicals Responsible for Bacterial Neuraminidase Inhibition and Their Characterization by UPLC-ESI-TOF/MS. *Food Funct.* **2022**, *13* (13), 6923−6933.
(34) Shah, A. B.; Baiseitova, A.; Kim, J. H.; Lee, Y. H.; Park, K. H. Inhibition of Bacterial Neuraminidase and Biofilm Formation by Ugonins Isolated From *Helminthostachys Zeylanica* (L.) Hook. *Front. Pharmacol.* **2022**, *13*, 10.
(35) Baiseitova, A.; Shah, A. B.; Kim, J. Y.; Ban, Y. J.; Kim, J. H.; Nafiah, M. A.; Park, K. H. O-Alkylated Quercetins with Selective Acetylcholinesterase and $\beta$-Secretase Inhibitions from *Melicope Glabra* Leaves, and Their Flavonols Profile by LC-ESI-Q-TOF/MS. *J. Funct. Foods* **2021**, *84*, 104602.
(36) Wiesmann, C.; Barr, K. J.; Kung, J.; Zhu, J.; Erlanson, D. A.; Shen, W.; Fahr, B. J.; Zhong, M.; Taylor, L.; Randal, M.; McDowell, R. S.; Hansen, S. K. Allosteric Inhibition of Protein Tyrosine Phosphatase 1B. *Nat. Struct. Mol. Biol.* **2004**, *11* (8), 730−737.
(37) Verdonk, M. L.; Cole, J. C.; Hartshorn, M. J.; Murray, C. W.; Taylor, R. D. Improved Protein-Ligand Docking Using GOLD. *Proteins* **2003**, *52* (4), 609−623.
(38) Bharatham, K.; Bharatham, N.; Kwon, Y. J.; Lee, K. W. Molecular Dynamics Simulation Study of PTP1B with Allosteric Inhibitor and Its Application in Receptor Based Pharmacophore Modeling. *J. Comput.-Aided Mol. Des.* **2008**, *22* (12), 925−933.
(39) Li, Z. P.; Lee, H.-H.; Uddin, Z.; Song, Y. H.; Park, K. H. Caged Xanthones Displaying Protein Tyrosine Phosphatase 1B (PTP1B) Inhibition from *Cratoxylum Cochinchinense*. *Bioorg. Chem.* **2018**, *78*, 39−45.


https://doi.org/10.1021/acsomega.3c07471
*ACS Omega* 2024, 9, 9053−9062